

Advanced biodiversity monitoring for results-based and effective agricultural policy and transformation

Deliverable D2.3
Remote sensing biodiversity indices ready for validation/demonstration

Due date of deliverable: 31st of January 2025

Actual submission date: 30th of January 2025



**Funded by
the European Union**

Funded by the European Union. Views and opinions expressed in this document are however those of the authors only and do not necessarily reflect those of the European Union or of the European Research Executive Agency. Neither the European Union nor the granting authority can be held responsible for them.

GENERAL DATA

Grant Agreement: Project 101081964

Project acronym: BioMonitor4CAP

Project title: Advanced biodiversity monitoring for results-based and effective agricultural policy and transformation

Project website: www.biomonitor4cap.eu

Start date of the project: December 1st, 2022

Project duration: 48 months

Organisation name of lead contractor: LEIBNIZ-INSTITUT ZUR ANALYSE DES BIODIVERSITAETSWANDELS

Call: HORIZON-CL6-2022-BIODIV-01

Topic: HORIZON-CL6-2022-BIODIV-01-06

Type of action: HORIZON Research and Innovation Actions

DELIVERABLE NUMBER: D2.3

DELIVERABLE TITLE: Remote sensing biodiversity indices ready for validation/demonstration

DELIVERABLE TYPE: Report

WORK PACKAGE N: WP 2

WORK PACKAGE TITLE: Developing, testing and calibrating farmland biodiversity monitoring

DELIVERABLE LEADER: S4G

AUTHOR: Luis Figueroa, Tina Nikaein, Liliana Gonzalez, Ramadhan Ramadhan

CONTRIBUTORS: Daniel Dalton, Asef Darvishi, Stefan Ruess

REVIEWERS: Eva Niephaus, Paul Jarick, Gernot Paulus, Christoph Scherber, Vanessa Berger

DISSEMINATION LEVEL: PU



History of changes		
Version	Publication Date	Change
0.1	10/10/2024	First Draft
1.0	30/01/2025	Final version



DISCLAIMER

Funded by the European Union. Views and opinions expressed in this document are however those of the authors only and do not necessarily reflect those of the European Union or of the European Research Executive Agency. Neither the European Union nor the granting authority can be held responsible for them.



Table of Contents

Executive summary	6
1. Introduction	7
2. Satellite Remote Sensing	9
2.1 Method & Processing	9
2.2 Ecosystem Function	10
2.3 Ecosystem Structure	14
3. UAS Remote Sensing	17
3.1 Methods & Processing	17
3.2 Community Composition	21
3.3 Ecosystem Structure	21
3.4 Ecosystem Function	22
4. Additional Remote Sensing Products	23
5. Future Work	24
5.1 Expanding Biodiversity Metrics & Indicators	25
5.2 Ground-Truth Data Correlation Analyses	25
5.3 Drone Biodiversity Metrics & Indicators	26
References	28
Annex	32



Executive summary

This preliminary report presents the initial findings and methodologies for developing biodiversity metrics and indices using remote sensing technologies in agrobiodiversity landscapes. It aligns with **Milestone 4 (M4)** and **Task 2.2**, which focus on the integration of optical, radar, drone-mounted, and satellite data to map landscape parameters related to biodiversity. The indices have been automated and generated for select datasets, with further refinement and expansion planned over the next two years.

The report outlines key activities undertaken, including the application of remote sensing techniques to characterize landscape variability (e.g., structural and species diversity), the development of predictive models, and the creation of meaningful indices at spatial scales such as farms and habitats. While historical records have been integrated with Earth observation data, **no correlation analyses with ground-truth data have been performed yet**. This validation and calibration process will be a priority in upcoming project phases.

Tasks addressed in this report include:

- **Task 2.1:** Methods for monitoring biodiversity at the farm scale.
- **Task 2.2:** Assessment of remote sensing methods for biodiversity monitoring at larger scales.
- **Task 2.3:** Calibration and validation of predictive models.
- **Task 2.4:** Design of an easy-to-use biodiversity monitoring system.

These efforts aim to develop a robust indicator system that combines remote sensing-based biodiversity indices (T2.2) with in-situ indicators (T2.1) into a unified and interoperable framework (T2.3 and T2.4). The preliminary work detailed here lays the foundation for achieving this goal by providing automated outputs and insights into using remote sensing data for biodiversity assessment. Further work will include correlation analyses, additional index development, and user-oriented system validation.



1. Introduction

Agricultural intensification is widely recognized as a significant contributor to biodiversity loss, with the widespread adoption of mechanised and chemical-based farming practices leading to substantial environmental degradation (Lécuyer et al., 2021). With global food production projected to increase by 70% between 2000 and 2050, addressing this challenge is critical to halting terrestrial biodiversity loss, particularly in the context of international commitments like the 2030 Sustainable Development Goals and the Convention on Biological Diversity (CBD) Global Biodiversity Framework. Achieving these targets requires the urgent development of effective monitoring tools for biodiversity hotspots (Vanbergen et al., 2020).

The challenge of tracking biodiversity change is multi-faceted and has confounded various fields of study. This complexity arises from the diverse taxonomic scales at which biodiversity can be measured. Early endeavors to comprehend biodiversity largely revolved around the study of individual flora and fauna populations within specific landscapes (Reddy, 2021). Traditional methods revolve around specific populations that serve as proxies to better understand biodiversity as a whole (e.g., bird point-counts). It is crucial to recognize that changes in biodiversity operate at various spatial and temporal scales, making them amenable to monitoring through remote sensing technologies that encompass a wide array of biodiversity-related measures.

In response to the loss of biodiversity at regional scales, the Group on Earth Observations Biodiversity Observation Network (GEO BON) has introduced the concept known as essential biodiversity variables (EBVs). These variables aim to create a standardised framework for understanding and quantifying different aspects of biodiversity, ensuring a common language and set of parameters for monitoring biodiversity using remote sensing technologies (Pereira et al., 2013; Skidmore et al., 2021).

The BioMonitor4CAP project embraces this framework, aiming to harness remote sensing technologies to develop biodiversity monitoring tools tailored to agricultural landscapes. By linking remote sensing products to relevant EBVs, the project seeks to create a scalable, reproducible methodology for tracking biodiversity changes at multiple spatial and temporal scales. These efforts focus on generating open-source remote sensing products that can inform biodiversity conservation strategies and sustainable agricultural practices.

Our selection of remote sensing products stems from an extensive literature review conducted as part of Deliverable 1.2 (see *Annex 10*). This review identified the most relevant biodiversity indicators for agricultural landscapes, aligning with the EBV framework's categories and thematic areas. Specifically, our work has focused on indicators related to Ecosystem Function and Ecosystem Structure.

Indicators within the Ecosystem Function class are particularly valuable for understanding key processes such as photosynthetic activity, vegetation dynamics, and soil water content. These factors directly influence the ability of agricultural landscapes to sustain biodiversity and provide essential ecosystem services.



Meanwhile, indicators in the Ecosystem Structure class provide critical insights into the spatial organization and physical characteristics of ecosystems. They are essential for assessing habitat integrity and resilience, identifying patterns of land use and fragmentation, and tracking changes in vegetation coverage over time.

When developing these products, we placed significant emphasis on ensuring their scalability and reproducibility across a wide range of geographic areas. To achieve this, the products are generated using open-source data and software. The project comprises three core tasks:

1. **Scientific Literature Review:** As part of Deliverable 1.2, the project conducted a comprehensive review of recent research on biodiversity and remote sensing, outlining a selection of appropriate indicators derived from drone and satellite remote sensing.
2. **Selection of Remote Sensing Products:** Based on the literature review and the project's requirements, the most relevant remote sensing products were identified. These products encompass EBV-related indicators, including ecosystem function and ecosystem structure.
3. **Automated Product Generation:** Task 2.2 developed and implemented code to automate the generation of satellite remote sensing products on a quarterly basis. Drone measurements were done seasonally across selected research sites; products from multiple sensors were generated.



2. Satellite Remote Sensing

The generation of biodiversity-related remote sensing products has been accomplished by using the SNAP toolbox (Weiss, 2016), which generates biophysical products from Sentinel-2 TOC reflectance values. The toolbox employs an artificial neural network trained on the PROSAIL database; the input it requires comes from normalised values from the spectra found in the visible, near-infrared, shortwave infrared, and zenith and azimuth angles of Sentinel-2 imagery.

This framework produces key biophysical outputs, including leaf area index (LAI), fraction of absorbed photosynthetically active radiation (fAPAR), fraction of vegetation cover (FVC), chlorophyll content, and canopy water content. Chlorophyll content in the canopy (CCC) is further calculated as a product of Cab (chlorophyll content per unit leaf area) and LAI, offering insights into vegetation health and productivity.

2.1 Method & Processing

The process of generating biophysical outputs involves several steps that utilize Sentinel-2 satellite imagery and Python-based tools. The example script provided (see *Annex 15*) demonstrates a workflow that combines data retrieval through the Microsoft Planetary Computer STAC API and processing with libraries such as Rasterio, NumPy, and Geopandas.

First, the method starts by defining a region of interest (ROI) using a GeoJSON file that outlines the spatial boundaries. This ROI corresponds to the grids that have been used during fieldwork campaigns; a 10-kilometer buffer around these grids has been calculated to include the surrounding landscape. The script reads the file using Geopandas and calculates the bounding box for the area, which serves as an input parameter for querying the STAC API. The script then connects to Microsoft Planetary Computer by creating a STAC client which then queries a request to the Sentinel-2 Level-2A collection with a specific temporal range and the previously defined spatial boundaries.

Once the data are retrieved, the script selects the first available item in the collection and extracts relevant metadata, including solar and viewing angles of the sensor, which are essential for accurate biophysical computations. The script identifies the necessary Sentinel-2 bands for each calculation (e.g., LAI), including spectral bands from different wavelengths (i.e., B03, B04, B05, B06, B07, B08A, B11 and B12). These bands are then read as a raster dataset using Rasterio and stored in a stack format for further processing.

The final values are computed by combining the neuron outputs through a final equation representing the model's last layer. These values are then denormalized to convert them back into the original physical range of the biophysical parameter. If specified in the configuration, the output is scaled by a division factor to meet specific unit requirements. This process produces raster layers representing biophysical values for the defined ROI on a quarterly basis. This quarterly schedule aligns with the dates of in-situ data collection, ensuring seamless integration of remote sensing and ground-based observations.

To generate these remote sensing products, we utilized the Google Earth Engine (GEE) collections 'COPERNICUS/S2_SR_HARMONIZED' and 'GOOGLE/CLOUD_SCORE_PLUS/V1/S2_HARMONIZED'



(Sentinel-2 based) to create composite images. These composites, derived from multiple images within each quarterly period (i.e., Jan-Mar, Apr-Jun, Jul-Sep, Oct-Dec) of 2023 and 2024, were spatially aggregated using the median to reduce noise, with a cloud threshold of 0.6 to exclude cloud-covered pixels. These Sentinel-2 composites provided the foundation for deriving various vegetation indices and texture features. Similarly, Sentinel-1 data from the GEE collection 'COPERNICUS/S1_GRD' was used to create quarterly radar-based composites, also aggregated using median values, to calculate radar vegetation indices.

The timing and methods used for in-situ data collection are detailed in the tables included in the Annex section. These tables summarize the specific devices, dates, and locations of in-situ measurements, providing a clear link between field data collection and the derived remote sensing products.

True Color (Red/Green/Blue) and False Color (Near-Infrared/Red/Green) composites were included as part of the layers primarily for visualization purposes. True Color images utilize the red, green, and blue bands to produce images resembling what the human eye perceives, while False Color images utilize a combination of near-infrared, red, and green bands. The inclusion of the near-infrared channels shows vegetation in different shades of red, with brighter red colour indicating healthier vegetation. Areas with bare soil or low vegetation can be seen in colours ranging from white to greens and browns, water surfaces appear in shades of blue to black colours, and clouds or snow are represented in white colour. This makes False Color images useful for providing insights into plant health and performing land cover classification, determining water boundaries, monitoring deforestation, tracking crop and forest harvest, and other applications (University of North Carolina, Institute of the Environment, n.d).

2.2 Ecosystem Function

The **normalized difference vegetation index (NDVI)** is calculated as the ratio of the difference between the measured canopy reflectance in the red and near-infrared bands (Gandhi et al., 2015). This parameter is used to quantify the productivity and above-ground biomass of ecosystems and can provide estimates of primary productivity, which has been shown to effectively predict regional variations in species richness (Parviainen et al., 2010; Gould, 2000). NDVI values range from -1 to 1, with areas having values <0.1 typically represents bare soils, rock, sand, or snow. Values between 0.2 to 0.5 often indicate sparse vegetation and values between 0.6 to 0.9 show dense vegetation (U.S. Geological Survey, 2018). Areas with low NDVI indicate the absence of vegetation or moisture-stressed vegetation, while a higher value suggests abundant and healthy vegetation (Parviainen et al., 2010; Tucker, 1979).

$$NDVI = \frac{NIR - RED}{NIR + RED}$$

The **normalized difference moisture index (NDMI)** measures vegetation moisture content by comparing the near-infrared and short-wave infrared bands (*Table 1*). This index can detect water stress at an early stage and provides insights into plant water content, which can be correlated with phenological development (Berca & Horoias, 2022). NDMI values range from -1 to 1 and can be interpreted as follows:



Table 1. NDMI Value Interpretation Table

<i>NDMI value</i>	<i>Interpretation</i>
< -0.8	Bare soil
-0.8 to -0.6	Almost absent vegetation
-0.6 to -0.4	Very reduced vegetation
-0.4 to -0.2	Low and dry vegetation
-0.2 to 0	Medium-low vegetation cover with high water stress
0 to 0.2	Medium-low vegetation cover with low water stress
0.2 to 0.4	Medium vegetation cover with low water stress
0.4 to 0.6	High vegetation cover with no water stress
0.6 to 0.8	Very high vegetation cover with no water stress
0.8 to 1.0	Total vegetation cover with no water stress

$$NDMI = \frac{NIR - SWIR}{NIR + SWIR}$$

The **leaf area index (LAI)** is a dimensionless measure representing the total one-sided leaf area per unit ground area. It is an indicator of plant canopy structure and ecosystem productivity. As such, LAI is classified under the EBVs of both ecosystem structure and ecosystem function. It is directly linked to ecosystem processes such as primary productivity, carbon sequestration and net ecosystem exchange (Fang et al., 2019). LAI is calculated using remote sensing data by analyzing the interaction of vegetation with incoming solar radiation.

Remote sensing platforms like MODIS and Sentinel-2 estimate LAI by combining spectral data (e.g., red and NIR bands) with radiative transfer models or neural network algorithms. MODIS provides global LAI products at a resolution of 500m, while Sentinel-2, with its finer spatial resolution (10–20m), enables localised assessments suitable for agricultural and ecological studies (*Figure a*).



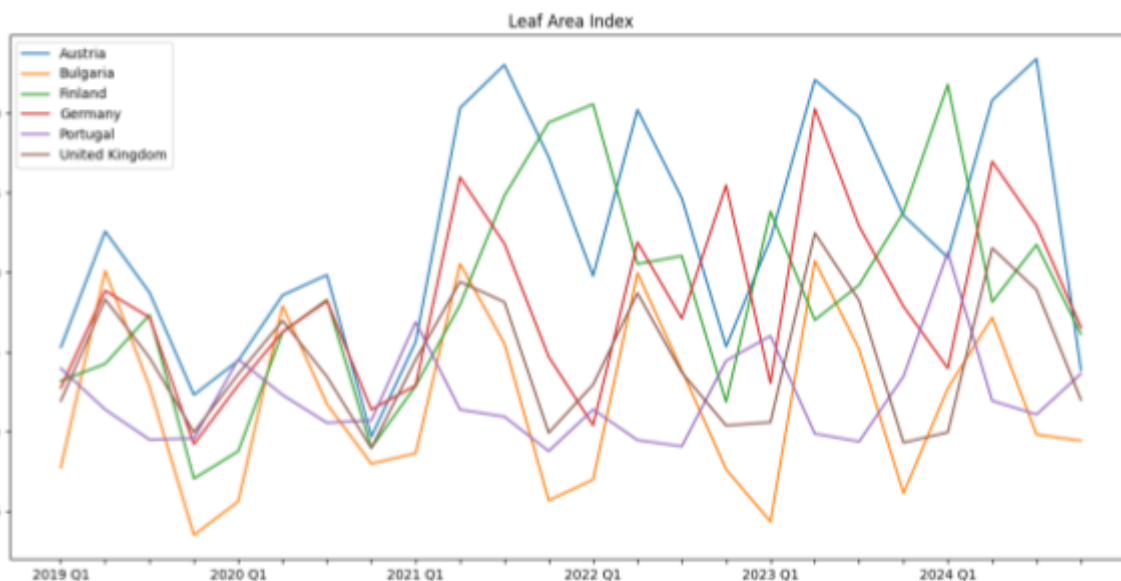


Figure a. LAI Trends for Major Research Sites (2019 - 2024)

The **fraction of absorbed photosynthetically active radiation (fAPAR)** is the proportion of solar radiation absorbed by vegetation for photosynthesis. As a biophysical variable, it explains ecosystem productivity and health. fAPAR falls under the ecosystem function EBV class since it reflects the density, health, and distribution of vegetation which hosts biodiversity. By quantifying how much energy plants absorb, fAPAR provides insights into primary productivity, habitat quality, and ecosystem resilience after landscape disturbances. This biophysical parameter is dimensionless, as it represents a fraction or ratio of absorbed to incoming solar radiation in the photosynthetically active radiation (PAR) range (400-700 nm); thus, values range from 0 to 1 (*Figure b*).

$$fAPAR = 1 - \frac{PAR_{notabsorbed}}{PAR_{absorbed}}$$

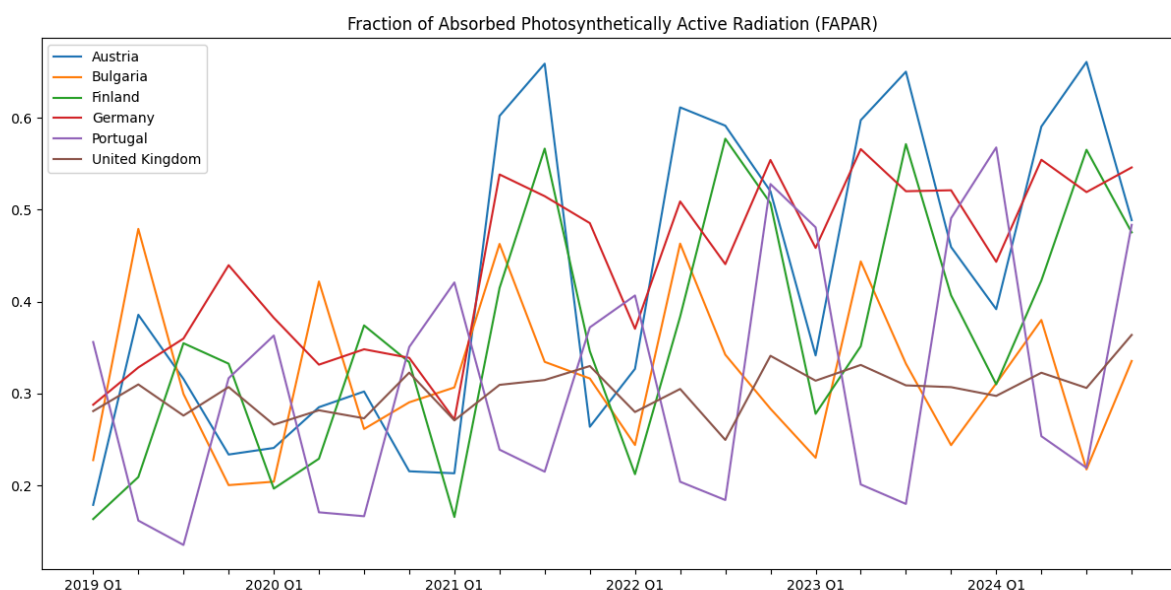


Figure b. fAPAR Trends for Major Research Sites (2019 - 2024)



fAPAR can be calculated from Sentinel-2 images using neural network algorithms like the NNET, which utilises the spectral bands with 10-meter spatial resolution. The algorithm relies on reflectance inputs from the visible, near-infrared, and shortwave infrared bands and auxiliary data like the sun and view zenith. The auxiliary inputs enhance the radiative transfer models underlying the neural network to perform the calculations. Higher fAPAR values indicate robust vegetation, while variations in fAPAR can signal ecosystem stress or habitat degradation.

Chlorophyll content is an indicator of plant health and stress, closely linked to nitrogen availability and photosynthetic efficiency, as noted by Houllès et al. (2007), and serves as a parameter in assessing ecosystem function, particularly under the EBV class of primary productivity. Chlorophyll content can be evaluated at two scales: the leaf level (Cab) and the canopy level (CCC). While Cab provides detailed information about individual leaves, CCC integrates this across the entire plant canopy.

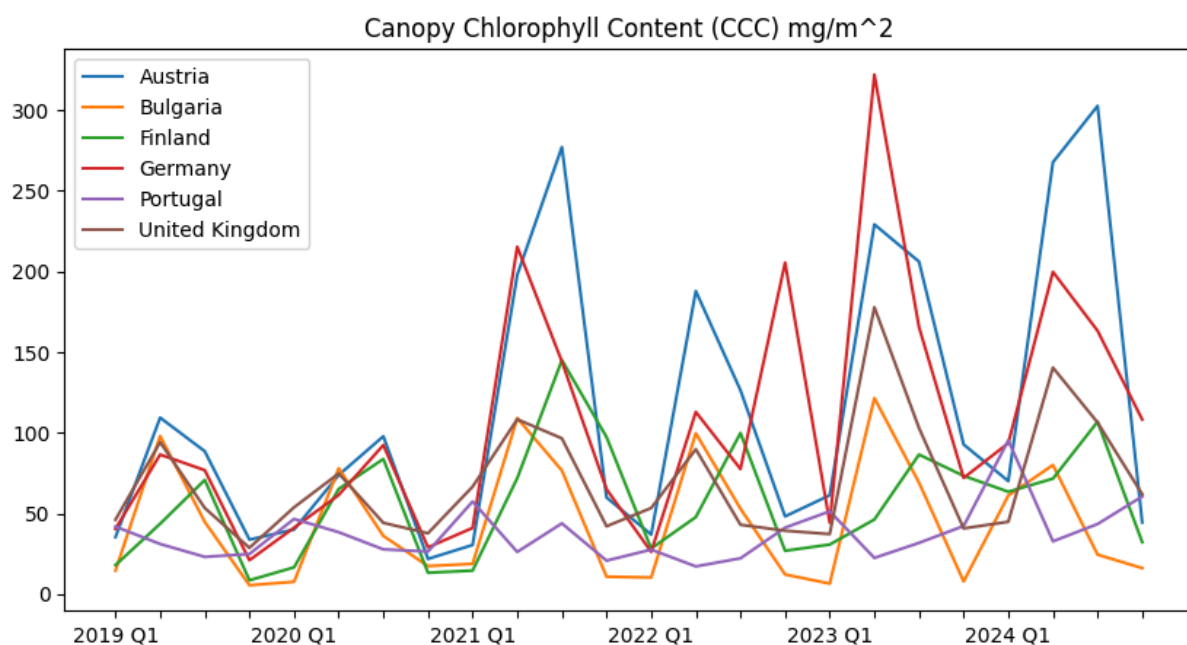


Figure c. CCC Trends for Major Research Sites (2019 - 2024)

CCC is calculated as the product of leaf chlorophyll content and LAI. Direct estimations of CCC have been demonstrated to be more robust and accurate than deriving it through separate estimations of Cab and LAI (Weiss et al., 2000). Studies that aim to model primary productivity in landscapes have relied on the use of CCC since it is strong at describing the photosynthetic efficiency of plants (Ali et al., 2021). The ability to directly estimate CCC from remote sensing data, using spectral indices and radiative transfer models, makes it a powerful tool for large-scale monitoring (Figure c). Recent advances in satellite missions such as Sentinel-2 and studies like those by Croft et al. (2020) and Campos-Taberner et al. (2018) underscore its application in understanding ecosystem dynamics and predicting vegetation responses to environmental changes.

Expected values for CCC vary depending on vegetation type and environmental conditions, but expected values should be from 0 to 600. CCC, being a composite measure, ranges widely depending



on canopy density and leaf chlorophyll levels, often expressed in milligrams of chlorophyll per square meter (mg/m^2).

Soil Moisture is considered a key driver of biodiversity and it is mostly related to ecosystem function; it can be estimated using Sentinel-1 radar imagery. The temporal dynamics and spatial distribution of soil moisture significantly influence biodiversity by regulating critical ecosystem processes. For instance, droughts can disrupt the relationship between biodiversity and ecosystem functioning, highlighting the importance of monitoring soil moisture as an ecological parameter (Lausch et al., 2019). By analyzing changes in radar backscatter intensity, variations in soil moisture can be detected, providing valuable insights into ecosystem health.

The estimation process involves calibrating relative changes in soil moisture to absolute values. Low soil moisture levels are set at approximately 0%, while wet soils are calibrated to around 60%. To enhance the accuracy of these calculations, the processing script excludes permanent water bodies and built-up areas (*Figure d*)

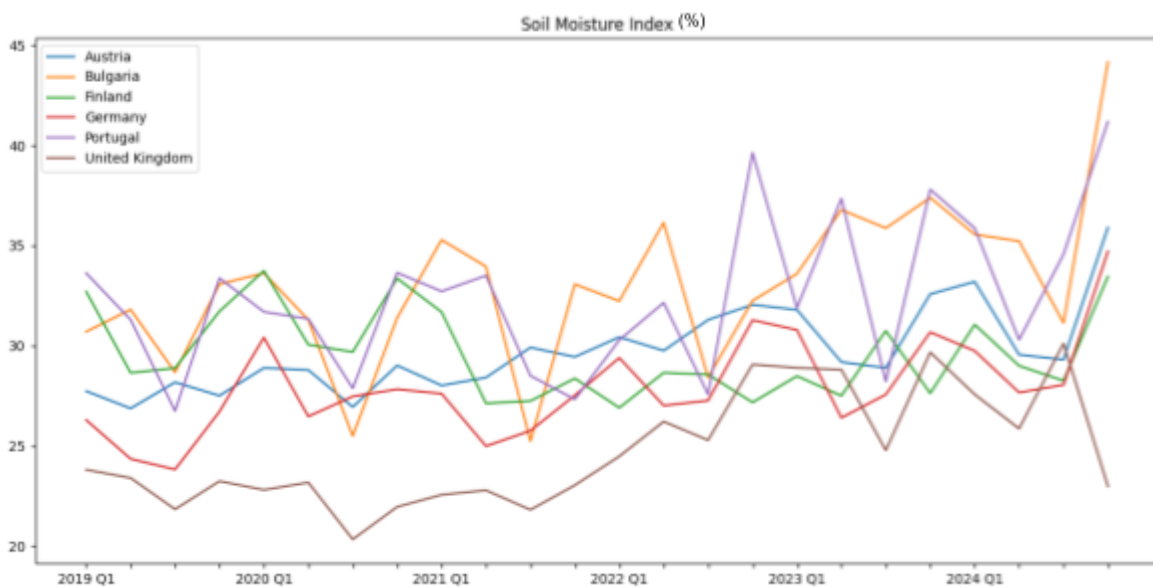


Figure d. Soil Moisture Index Trends for Major Research Sites (2019 - 2024)

2.3 Ecosystem Structure

Land cover is a key variable in environmental monitoring because it directly influences biodiversity, climate, and land use practices. Over the years, land cover mapping has seen significant advancements due to improvements in satellite imagery, computational techniques, and the development of global monitoring programs. We used two land cover sources: ESA Copernicus Global Land Cover Layers: CGLS-LC100 Collection 3 and Dynamic World Land Cover. Throughout the major research sites, land cover metrics have been obtained to track significant changes in the coverage (*Figure e*).



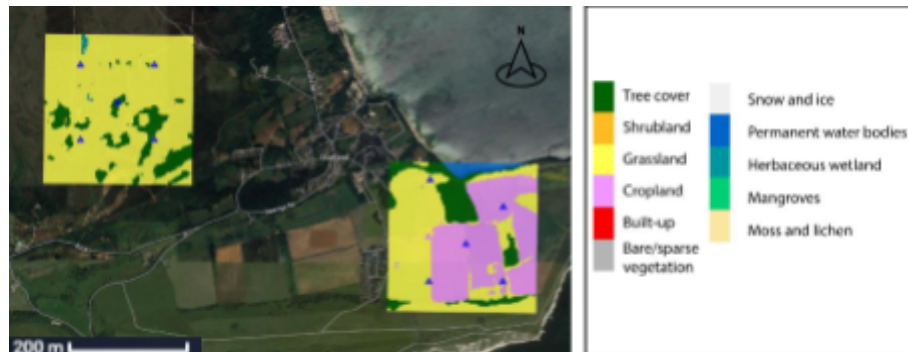


Figure e. Land Cover Classification of UK Grids Using CGLS

- ESA Copernicus Global Land Cover Layers: CGLS-LC100 Collection 3: This dataset from ESA provides detailed annual global land cover classifications starting from 2015 with a resolution of 100 meters. It is based on Proba-V satellite data and includes 23 classes defined by the Land Cover Classification System..
- Dynamic World Land Cover: Developed by Google Earth Engine and World Resources Institute, this system uses Sentinel-2 imagery to offer a near real-time view of global land cover at 10-meter resolution. It updates every 2-5 days, providing probabilistic land cover classifications across nine major categories.

Both datasets significantly enhance our capacity to track and understand EBVs. The detailed, frequent updates from Dynamic World Land Cover are ideal for monitoring short-term changes in ecosystems, such as those caused by natural disasters or seasonal variations. In contrast, the annual snapshots provided by CGLS-LC100 are invaluable for observing long-term trends in land cover, which are essential for assessing changes in habitat extent and quality, and by extension, biodiversity.

The **fraction of vegetation cover (FCOVER)** is a dimensionless measure representing the proportion of the ground surface covered by green vegetation. FCOVER falls under the EBV class Ecosystem Structure since it provides insights into plant density, vegetation growth and land cover changes. When combined with other indicators, it provides information used to assess biomass and primary productivity (Li et al., 2023).

Empirical or radiative transfer models are applied to translate reflectance measurements into FCOVER values. Neural network algorithms, similar to those used for estimating fAPAR and LAI, are also employed to enhance accuracy in deriving FCOVER from high-resolution satellite data such as Sentinel-2 or MODIS.

Unlike fAPAR, FCOVER is independent of the geometry of illumination, making it consistent across different sensors. It is susceptible to low cover fractions, making it a useful indicator for sparse vegetation or early vegetation growth stages. FCOVER ranges from 0 to 1, where 0 represents bare ground, and 1 corresponds to complete vegetation coverage of the surface (*Figure f*).



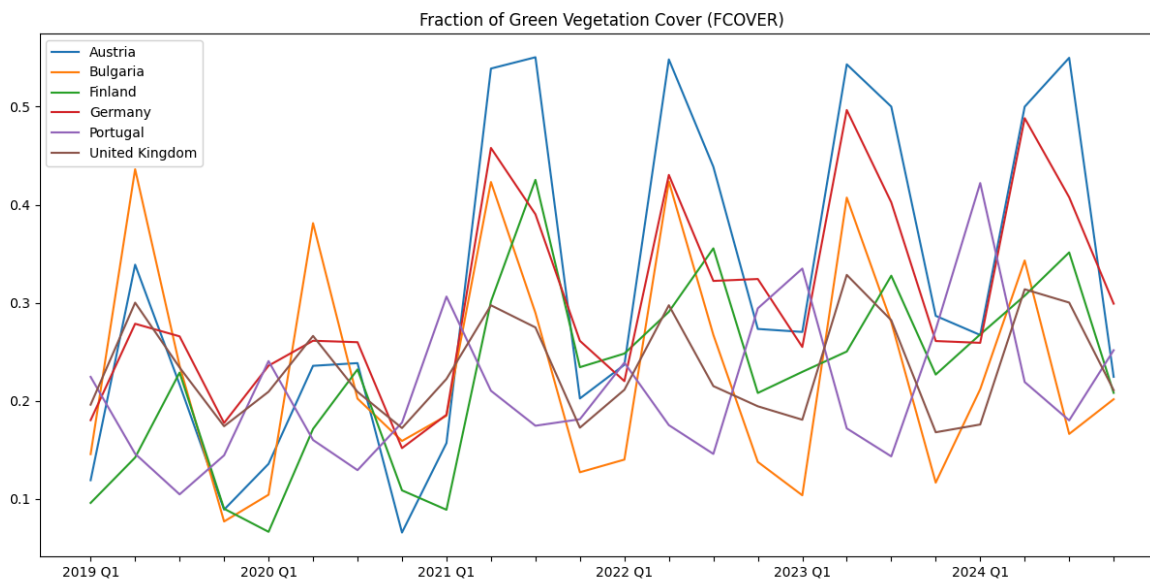


Figure f. Soil Moisture Index Trends for Major Research Sites (2019 - 2024)

The **gray-level co-occurrence matrix (GLCM)** is a widely used texture analysis technique that quantifies spatial relationships between pixel intensities in an image. GLCM evaluates how often pairs of pixel values with specific spatial relationships (e.g., distance and orientation) occur in an image. It generates a matrix where each element represents the frequency of a specific pixel pair, which can then be used to compute various statistical texture metrics such as:

- **Contrast:** Measures the intensity difference between a pixel and its neighbor.
- **Homogeneity:** Reflects how similar pixel values are across an area.
- **Energy:** Indicates the uniformity or repetition of patterns.
- **Entropy:** Represents the randomness or complexity in pixel values.

These texture features are derived from multispectral imagery. They provide information beyond simple spectral reflectance, offering insights into the spatial structure and complexity of land cover and vegetation.

GLCM-derived texture metrics can describe vegetation structure, a critical aspect of EBVs related to ecosystem composition and configuration. GLCM features like **contrast** and **homogeneity** quantify the heterogeneity or uniformity of vegetation cover. These metrics are proxies for canopy complexity, which is directly linked to habitat suitability for various species. GLCM can support functional EBVs by revealing patterns related to vegetation productivity and water use. Texture metrics can track changes in vegetation texture over time, reflecting seasonal growth, senescence, or disturbances. This temporal variation links to ecosystem productivity and nutrient cycling. Spatial patterns revealed by GLCM metrics, such as high entropy or contrast, are often linked to species richness, habitat diversity, and ecosystem health.



3. UAS Remote Sensing

Agricultural activities are major drivers affecting habitat and species diversity in agroecosystems. Monitoring biodiversity in such landscapes is one of the most important tasks to make informed management decisions to prevent biodiversity loss. Our study objective is to identify and develop new biodiversity monitoring indicators to establish a methodological framework for biodiversity monitoring. In this regard, uncrewed aerial systems (UAS) technology offers significant contributions at low cost. The diversified temporal and spatial frequency of UAS flight campaigns at field and farm scales is suited to address limitations of detail inherent in satellite imagery.

3.1 Methods & Processing

To capture high-resolution data for biodiversity monitoring, our UAS are equipped with two sensor systems: an RGB camera and a multispectral sensor. Together, these systems provide complementary datasets that can be used for analyzing ecological variables within the ROI. Images are first gathered and subsequently analyzed using Metashape software (Agisoft, St. Petersburg, Russia). In the context of biodiversity, we identify landforms, vegetation indices, and landscape composition. The high-resolution imagery allows analysis of features related to the EBV classes Ecosystem Function, Ecosystem Structure and Community Composition. *Annex 11, 12, 13, and 14* (See Annex section) provide flight information from flight campaigns at the Leibniz Innovation Farm for Sustainable Bioeconomy, InnoHof.

The RGB sensor enables ground-truthing, validating field measurements, and integrating data from other sources. This sensor captures imagery from the visible light spectrum, producing detailed, True Color representations of the landscape. True Color imagery allows visual analysis for species identification, counting of plant inflorescences, and a general assessment of landscape features. Additionally, this type of imagery is used to generate orthomosaics—high-resolution, geo-referenced maps that support highly detailed spatial analysis. By employing photogrammetry, the RGB camera also contributes to assessing structural complexity, revealing physical habitat characteristics such as vegetation density and spatial distribution patterns.

The multispectral sensor, on the other hand, captures spectral information beyond visible light to capture data across additional wavelengths, including near infrared and red edge wavelengths. This capability is essential for understanding vegetation health and ecological variability. The sensor enables the calculation of vegetation indices, such as NDVI, highlighting patterns in vegetation health and density that cannot be observed by the human eye. It also enhances the detection of floral regions by leveraging distinct spectral signatures, improving the accuracy of flower mapping and habitat characterization. By differentiating plant species and capturing spatial variability in vegetation composition, the multispectral sensor provides deeper insights into habitat structure. Furthermore, its capacity for repeated measurements makes it ideal for studying seasonal changes and monitoring habitat dynamics over time.



UAS Data Collection Missions: Austria

In BioMonitor4CAP, UAS missions were executed at different locations in Carinthia, Austria. In June and September 2023, test missions were conducted at a study site near Klagenfurt. In 2024, 10 missions were performed overall across two sites near Klagenfurt and a third site in the district of Feldkirchen. *Table 2* shows the respective mission dates, the used platforms and sensors, and the resulting raw data.

Table 2. Overview of UAS and GCP Data Collection Campaigns

Date	Data Collection	Platform	Sensor	Georeferencing RMSE	Raw Data	Data Format
2024-03-08	UAS Dormant	DJI M 350 RTK	DJI P1, Micasense Dual	1.05	Orthomosaic RGB, Ortho multispectral, DSM, 3D Point Cloud	Raster data; GeoTIFF Point Cloud: .las
2024-03-14	UAS Dormant	DJI M 350 RTK	DJI P1, Micasense Dual	1.65	Orthomosaic RGB, Ortho multispectral, DSM, 3D Point Cloud	Raster data; GeoTIFF Point Cloud: .las
2024-03-29	GCP	Leica GNSS	Leica RTK	n/a no flight due to poor weather	GCPs established	.txt
2024-04-05	UAS	DJI M 350 RTK	DJI P1, Micasense Dual	1.54	Orthomosaic RGB, Ortho multispectral, DSM, 3D Point Cloud	Raster data; GeoTIFF Point Cloud: .las
2024-05-25	UAS	DJI M 350 RTK	DJI P1, Micasense Dual	2.58	Orthomosaic RGB, Ortho multispectral, DSM, 3D Point Cloud	Raster data; GeoTIFF Point Cloud: .las
2024-06-28	UAS	DJI M 350 RTK	DJI P1, Micasense Dual	1.82	Orthomosaic RGB, Ortho multispectral, DSM, 3D Point Cloud	Raster data; GeoTIFF Point Cloud: .las
2024-07-16	UAS	DJI M 350 RTK	DJI P1, Micasense Dual	1.85	Orthomosaic RGB, Ortho multispectral, DSM, 3D Point Cloud	Raster data; GeoTIFF Point Cloud: .las
2024-09-17	UAS	DJI M 350 RTK	DJI P1, Micasense Dual	0.72	Orthomosaic RGB, Ortho multispectral, DSM, 3D Point Cloud	Raster data; GeoTIFF Point Cloud: .las
2024-09-18	UAS	DJI M 350 RTK	DJI P1, Micasense Dual	2.24	Orthomosaic RGB, Ortho multispectral, DSM, 3D Point Cloud	Raster data; GeoTIFF Point Cloud: .las
2024-09-20	UAS	DJI M 350 RTK	DJI P1, Micasense Dual	1.45	Orthomosaic RGB, Ortho multispectral, DSM, 3D Point Cloud	Raster data; GeoTIFF Point Cloud: .las
2024-11-29	UAS	DJI M3E	M3E	n/a no GCPs used, RTK correction enabled	Orthomosaic RGB, DSM, 3D Point Cloud	Raster data; GeoTIFF Point Cloud: .las

The data collection missions progressed from UAS-based image acquisition to photogrammetric processing, ultimately producing analysis-ready datasets for each timestamp. Field measurements were conducted to establish ground control points (GCPs) necessary for georeferencing the data. Georeferencing is a critical step in remote sensing, particularly when comparing raster datasets from



different sensors and timestamps or performing change detection. This process involves defining the raster data's location using WGS84 coordinates, which are then employed to assign the coordinate system of the map frame (ESRI, 2024). The control points, which can be accurately identified within the raster data, were measured in the field using a global navigation satellite system (GNSS) device.

These control points were transformed over a local fixed-point network, allowing the WGS84 coordinates from the GNSS to be converted into MGI / Austria GK Central (EPSG 31255) coordinates. By using the projected and measured GCPs, the raster data were shifted and warped from the original locations to the spatially corrected location (ESRI, 2024). The primary device used for GCP data collection was the Leica Viva GS16 GNSS Rover (Leica Geosystems, St. Gallen, Switzerland). These measurements were crucial for georeferencing the photogrammetric processing results and transforming them into the appropriate projected coordinate system. The GCPs were strategically placed across each study site to encompass varying topographic levels, including areas above and below steep slopes (*Figure g*). RGB and multispectral data were collected during the missions. An automated flight plan was employed for data collection, ensuring 80% forward image overlap and 90% side overlap. *Table 3* details the different flight parameters from the Austrian UAS missions.



Figure g. Collecting GCP measurements at the study site Winkl, district of Feldkirchen, Carinthia, Austria using the Leica GS16 GNSS Rover



Table 3. UAS Flight Parameters for Carinthia, Austria

Parameter	Value
Flight Speed	4 m/s
Altitude (above ground level)	80m
Sensor orientation	Nadir
Ground Sampling Distance GSD	1 cm RGB / 7 cm multispectral
Georeferencing error	Mean 1.65 cm
Side overlap	90 %
Forward overlap	80 %
Shooting style	1 img / 2 sec

The UAS DJI M350 RTK (SZ DJI Technology Co., Ltd., Shenzhen, Guangdong, China), equipped with two sensors, was utilized for data acquisition (*Figure h*). High-resolution RGB imagery was captured using DJI's P1 RGB full-frame sensor, which delivers a spatial resolution of 40 megapixels. Multispectral imagery was collected with the Micasense RedEdge-Dual sensor (Micasense Inc., Seattle, WA), capable of recording data across 10 spectral bands at a spatial resolution of 7 cm.



Figure h. The DJI M350 RTK is equipped with a Micasense dual (viewed from the front) on the left and a DJI P1 RGB camera mounted on the right. Both sensors are triggered at the same time.

Key spectral bands included blue (475 nm), green (560 nm), and red (668 nm) within the visible spectrum, as well as red edge (717 nm) and near infrared (NIR) (840 nm). To ensure data accuracy, the multispectral sensor was calibrated using the reference panels supplied with the device, following the protocol outlined by Daniels et al. (2023). At the beginning and at the end of each mission, a calibration panel is photographed with the Micasense sensor. The calibration images were later used in Metashape Version 1.8 for the automated radiometric calibration of the multispectral data where each channel's reflectance value was scaled based on the captured lighting conditions.

A photogrammetric workflow was implemented to process the data collected during UAS missions, producing georeferenced orthomosaics, digital surface models (DSMs) and dense point clouds of the



study sites. These missions were complemented by the measurement of GCPs for georeferencing. The data processing was carried out using Structure-from-Motion with Metashape software, a method designed for generating 3D spatial datasets. The initial step involved visualizing the data to ensure sufficient coverage of the research site (Agisoft, 2023). Resulting images were stored and aligned by identifying matching points between images. This alignment process utilizes the interrelations between images to spatially orient them, resulting in a sparse point cloud (Westoby et al., 2012). The software automatically calculates the camera positions during this stage. After generating tie points, the alignment was optimized, georeferencing was performed, and a dense point cloud was generated.

The root mean error between the input GCP locations and their estimated positions was calculated as 1.65 cm across all survey missions. This total error was computed as the RMSE of all input GCP locations relative to their estimated positions (Agisoft, 2023). The dense point clouds were generated by connecting matching points from individual images and incorporating depth information. The resulting dense clouds were reviewed for outliers, which were edited as necessary. Using the georeferenced dense point clouds, DSMs were generated, which then served as the foundation for creating georeferenced orthomosaics. The same processing steps were performed for both the RGB and the multispectral datasets. The respective outputs of the photogrammetric processing are shown in *Table 2*.

3.2 Community Composition

Community composition, a class of EBV describing the identity and abundance of species in an ecosystem, can be studied through remote sensing by linking spectral and spatial data to floral diversity, which in turn influences insect populations. High-resolution orthomosaics generated from RGB and multispectral drone imagery can identify flowering hotspots and species distribution. These maps can be correlated with insect diversity and abundance, particularly for pollinators like bees, which are highly dependent on floral resources (Torresani et al., 2023). Spectral signatures and vegetation indices, such as NDVI, can highlight areas of high productivity and floral density, serving as proxies for suitable habitats for pollinator communities. Similarly, camera trapping and bioacoustic monitoring at ground stations can validate UAS-based findings by providing insights into insect activity and diversity.

For birds, community composition is influenced by habitat-specific preferences, which can be indirectly assessed using remote sensing products like vegetation density maps, canopy height models, and habitat heterogeneity indices derived from UAS data (Santangeli et al., 2020). By identifying tree species, shrub densities, and open grasslands, UAS provide data that can be linked to bird species richness and nesting preferences.

3.3 Ecosystem Structure

Ecosystem structure, focusing on the physical arrangement of biotic and abiotic components, is a crucial EBV that can be explored using UAS-derived data. Structural complexity of habitats, such as vertical layering and vegetation density, plays a significant role in shaping the biodiversity of birds and insects (Torresani et al., 2024). High-resolution photogrammetry using RGB data enables the



generation of three-dimensional models that reveal canopy height, understory density, and habitat complexity. These models help identify nesting habitats for birds and microhabitats for insects.

3.4 Ecosystem Function

Ecosystem function, encompassing processes like productivity and nutrient cycling, can also be assessed using UAS-derived remote sensing products. Multispectral imagery enables the calculation of indices such as NDVI, enhanced vegetation index (EVI), and soil adjusted vegetation index (SAVI) (Fu et al., 2024). These indices provide insights into vegetation health and productivity, which directly impact insect populations that are dependent on floral and plant resources.



4. Additional Remote Sensing Products

This section explores remote sensing products that, while not neatly categorized within traditional EBVs like community composition, ecosystem structure, or function, nonetheless offer valuable insights into biodiversity. These products, identified through scientific literature, provide unique perspectives and contribute to a more comprehensive understanding of biodiversity.

One such product is the **burned area index for Sentinel-2 (BAIS2)**, which effectively detects burned areas by leveraging the short-wave infrared, red, and red edge spectral bands of Sentinel-2 data (Filipponi et al., 2018). BAIS2 values range from -1 to 1 for burn scars and from 1 to 6 for active fires. The index is calculated as follows:

$$BAIS2 = \left(1 - \sqrt{\frac{B06 * B07 * B8A}{B4}} \right) * \left(\frac{B12 - B8A}{\sqrt{B12 + B8A}} + 1 \right)$$

Where:

B4 = Red Band

B6 = Visible and Near Infrared band with central wavelength of 740nm

B7 = Visible and Near Infrared band with a central wavelength of 783nm

B8A = Visible and Near Infrared band with a central wavelength of 865nm

B12 = Short Wave Infrared band (SWIR)

Fires are recognized as a crucial factor in biodiversity monitoring due to their profound impact on ecosystems. They influence vegetation dynamics, habitat availability, and species distribution, making fire-related remote sensing products like BAIS2 invaluable for understanding biodiversity changes (Skidmore et al., 2021).

Beyond fire, **synthetic aperture radar (SAR)** provides valuable data for biodiversity assessment. SAR backscattered intensities, VV (vertical transmit and vertical receive) and VH (vertical transmit and horizontal receive) polarizations, along with the radar vegetation index (RVI), are highly sensitive to vegetation structure. These measures provide information on canopy density, biomass, and height, which are key components of ecosystem structure EBVs, including ecosystem vertical profile and habitat structure. They also contribute to ecosystem function EBVs, such as primary productivity and net ecosystem exchange.

$$RVI = \frac{4 \cdot \sigma_{VH}^0}{\sigma_{VV}^0 + \sigma_{VH}^0}$$

RVI is calculated based on VV and VH, with higher values generally indicating denser and more complex vegetation, while lower values suggest sparse vegetation or bare ground. The all-weather capabilities of SAR make these measures particularly useful for monitoring biodiversity in regions with frequent cloud cover. VV, VH, and RVI are valuable for assessing EBVs as they offer complementary data for monitoring ecosystem structure and function (*Figure i*). Their sensitivity to vegetation characteristics and all-weather capabilities make them indispensable for understanding and addressing biodiversity changes in the face of global challenges such as deforestation, climate change, and habitat loss (Schulz et al., 2024).



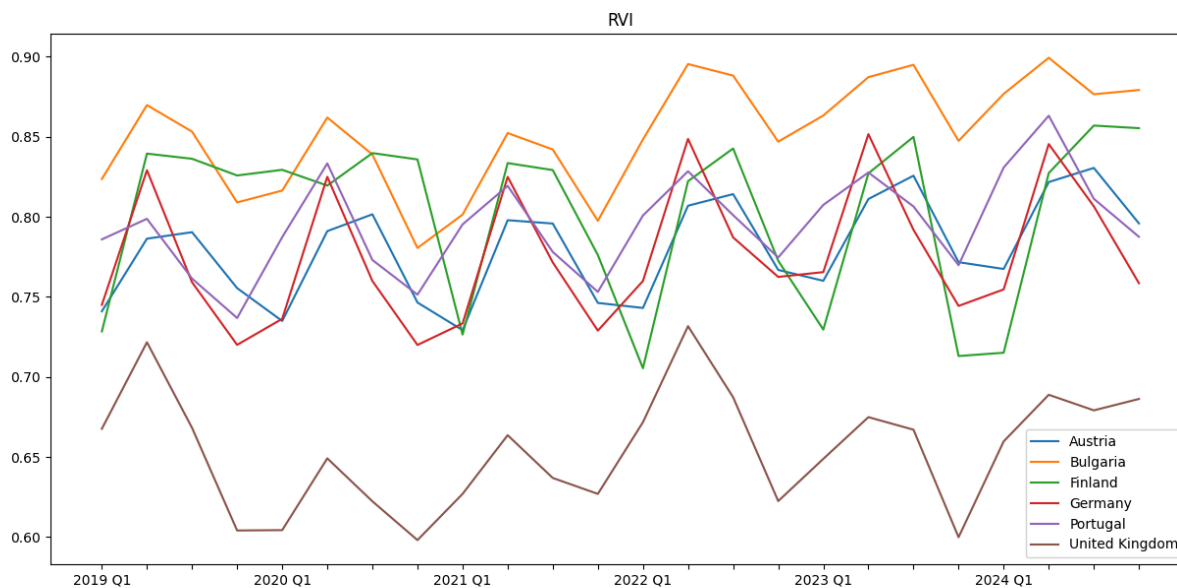


Figure i. RVI Trends for Major Research Sites (2019 - 2024)

Analyzing the coverage and distance to specific land cover types is crucial for understanding biodiversity. This approach involves assessing the amount of a particular land cover type within a given area and determining the proximity of a location to high-biodiversity land cover types, such as forests.

- **Distance to High-Biodiversity Land Cover:** This metric helps assess the potential influence of high-biodiversity areas on surrounding ecosystems. For example, the distance of a grassland area to the nearest forest edge can be a significant factor in determining the presence of forest-dependent species or the extent of edge effects. This can be calculated using distance functions in GIS software, with inputs being the location of the sampling station and a land cover map with the high-biodiversity land cover type identified.
- **Coverage of High-Biodiversity Land Cover:** Quantifying the proportion of high-biodiversity land cover within a given area provides insights into habitat availability and potential species richness. For instance, a higher percentage of forest cover within a grid cell might indicate greater habitat diversity that can support a wider range of species. This can be calculated by classifying the land cover within a grid cell and determining the proportion of the cell occupied by high-biodiversity land cover types.

Finally, **SoilGrids** layers provide maps of soil properties, including organic carbon, pH, texture, bulk density, and nutrient content. These properties are essential for understanding EBVs related to ecosystem composition, function, and structure. Soil organic carbon and texture influence biomass, vegetation growth, and habitat complexity, while pH and nutrient content regulate plant productivity, microbial activity, and nutrient cycling.



5. Future Work

Section 5 identifies two key areas for future work to enhance BioMonitor4CAP project outcomes. These areas include expanding the range of biodiversity indices and conducting thorough ground-truth data correlation analyses. By expanding the biodiversity indices, the project aims to develop novel indices tailored to agrobiodiversity, incorporating variables such as bioclimatic conditions, topographic features, and anthropogenic influences. Furthermore, the project seeks to address the limitations of existing remote sensing indices by incorporating high-resolution datasets and advanced remote sensing techniques.

5.1 Expanding Biodiversity Metrics & Indicators

Integrating remote sensing with in situ data collection offers a powerful approach to enhancing our understanding of biodiversity in agroecosystems. Increasing the spatial and temporal density of in situ biodiversity measurements across seasons and habitat types is crucial to capturing diverse ecological conditions (Schimel et al., 2019). This expanded dataset could support the development of biodiversity metrics beyond traditional indices, incorporating measures such as plant species diversity, insect populations, and ecosystem functionality (Jetz et al., 2019).

To address the limitations of existing remote sensing indices in reflecting complex ecological parameters, future research should focus on developing novel indices tailored to biodiversity. These could include variables such as bioclimatic conditions (e.g., temperature and precipitation), topographic features (elevation, slope, and aspect), and anthropogenic influences like proximity to roads (Gao et al., 2019). Incorporating high-resolution datasets such as the shuttle radar topography mission (SRTM) and global landform classification, alongside metrics like the high above nearest drainage (HAND) and forest or water body cover percentages, could provide deeper insights into ecological dynamics (Turner et al., 2018).

Advances in hyperspectral remote sensing may open new possibilities for detecting subtle spectral signals linked to biodiversity, such as vegetation chemical composition and soil microbial activity (Lausch et al., 2018). Time-series analyses of remote sensing data can also reveal temporal changes in vegetation and ecosystem conditions, offering a dynamic view of biodiversity trends (Pettorelli et al., 2018). These approaches align with recent studies emphasizing the need for high-resolution, temporally-rich datasets to advance biodiversity monitoring and conservation efforts (Skidmore et al., 2021; Turner et al., 2018).

5.2 Ground-Truth Data Correlation Analyses

The ground measurements conducted in 2023, which included assessments of bacterial and fungal diversities per grid point, failed to produce strong correlations with remote sensing layers. This outcome highlights several methodological and ecological challenges. A primary limitation was the sparse distribution of grid points per country, which likely proved inadequate for capturing the intricate biodiversity behaviours and ecological conditions present in the study regions. Similar studies have suggested that limited sampling densities often fail to reflect the full spectrum of biodiversity variability and environmental gradients (Helfenstein et al., 2022). This insufficiency



underscores the importance of carefully balancing spatial resolution and coverage when designing biodiversity monitoring frameworks.

The observed lack of correlation also underscores the inherent complexity of relationships between remote sensing variables and biodiversity metrics. These relationships are typically nonlinear and influenced by multiple interacting factors, including ecological dynamics, microclimatic variations, and anthropogenic pressures (Pettorelli et al., 2024). Addressing this complexity requires datasets with higher spatial and temporal granularity to capture these multifaceted interactions effectively. In 2024, over 1,000 grid points were sampled, marking a significant improvement in data collection efforts compared to 2023. Building on this progress, the plan for 2025 includes sampling an equal or greater number of points to further enhance coverage, capture regional variations, and reveal overarching patterns that were previously obscured by insufficient data.

Future research should prioritize leveraging advanced statistical techniques and machine learning approaches, such as nonlinear regression models, random forests, and neural networks, to analyze these expanded datasets. These methods are well-suited for identifying complex interactions and latent patterns within high-dimensional data, which traditional linear models often fail to detect (Lausch et al., 2018). For instance, machine learning frameworks have been successfully employed in previous studies to map biodiversity dynamics by integrating remote sensing indicators with ground-truth data, offering valuable insights into ecosystem functioning and conservation strategies (Antonelli et al., 2022).

5.3 Drone Biodiversity Metrics & Indicators

The RGB imagery collected during drone flights offers detailed, true color visual data that enable species identification and floral analysis at a fine spatial scale. Such data allow the development of species distribution models, mapping the presence and abundance of specific flora and fauna. Additionally, floral coverage can be quantified to assess habitat quality, supporting pollinators and other wildlife. Visible patterns in orthomosaics provide insights into habitat preferences, contributing to a better understanding of species richness and landscape biodiversity dynamics over time.

Photogrammetry techniques applied to RGB data enable the creation of three-dimensional models, revealing the structural complexity of habitats, including vegetation density and spatial arrangement. This information is vital for assessing habitat suitability for species and understanding interactions within ecosystems (Torresani et al., 2024). For example, dense vegetation may support nesting birds, while open understory benefits ground-dwelling species. Such structural insights also inform assessments of ecosystem resilience and recovery potential, which are critical for conservation planning.

Multispectral data captured by drones enhance this analysis by providing information beyond visible wavelengths. Indices such as NDVI enable monitoring of vegetation health and productivity, detecting stress caused by drought, pests, or human activity. Additional indices, including EVI and SAVI, offer complementary insights into vegetation dynamics (Fu et al., 2024). These metrics facilitate tracking of ecosystem productivity and identification of areas requiring restoration, making them especially valuable in agricultural landscapes.



The capacity for repeated multispectral measurements supports the study of seasonal and temporal changes in ecosystems. Seasonal changes in vegetation indices also provide critical information for pollinators and migratory species, ensuring conservation actions align with ecological cycles (Müllerová et al., 2025). Monitoring temporal trends further supports adaptive management by offering data on long-term ecosystem changes.

To provide a comprehensive understanding of biodiversity, drone-based metrics are integrated with station-level measurements such as environmental DNA (eDNA), bioacoustics, and soil parameters. For example, eDNA validates species presence detected through RGB imagery, while bioacoustic data complements fauna observations. Soil parameters, including moisture and nutrient levels, correlate with vegetation indices to uncover drivers of ecosystem productivity.



References

1. Agisoft. (2023). *Agisoft Metashape User Manual: Professional Edition*. In (Version Version 2.0) Agisoft LLC.
2. Ali, A. M., Abdullah, H., Darvishzadeh, R., Skidmore, A. K., Heurich, M., Roeoesli, C., Paganini, M., Heiden, U., & Marshall, D. (2021). Canopy chlorophyll content retrieved from time series remote sensing data as a proxy for detecting bark beetle infestation. *Remote Sensing Applications: Society and Environment*, *23*, 100524. <https://doi.org/10.1016/j.rsase.2021.100524>
3. Antonelli, A., Dhanjal-Adams, K. L., & Silvestro, D. (2022). Integrating machine learning, remote sensing and citizen science to create an early warning system for biodiversity. *People and Nature*, *4*(6), e10337. <https://doi.org/10.1002/ppp3.10337>
4. Berca, M., & Horoias, R. (2022). NDMI use in recognition of water stress issues, related to winter wheat yields in southern Romania. https://managementjournal.usamv.ro/pdf/vol.22_2/Art12.pdf
5. Campos-Taberner, M., Moreno-Martínez, Á., García-Haro, F. J., Camps-Valls, G., Robinson, N. P., Kattge, J., & Running, S. W. (2018). Global estimation of biophysical variables from Google Earth engine platform. *Remote Sensing*, *10*(8), 1167. <https://doi.org/10.3390/rs10081167>
6. Croft, H., Chen, J. M., Wang, R., Mo, G., Luo, S., Luo, X., He, L., Gonsamo, A., Arabian, J., Zhang, Y., Simic-Milas, A., Noland, T. L., He, Y., Homolová, L., Malenovský, Z., Yi, Q., Beringer, J., Amiri, R., Hutley, L., ... Bonal, D. (2020). The global distribution of leaf chlorophyll content. *Remote Sensing of Environment*, *236*, 111479. <https://doi.org/10.1016/j.rse.2019.111479>
7. Daniels, L., Eeckhout, E., Wieme, J., Dejaegher, Y., Audenaert, K., & Maes, W. H. (2023). Identifying the Optimal Radiometric Calibration Method for UAV-Based Multispectral Imaging. *Remote Sensing*, *15*(11). <https://doi.org/10.3390/rs15112909>
8. ESRI. (2024). Overview of Georeferencing. <https://pro.arcgis.com/en/pro-app/latest/help/data/imagery/overview-of-georeferencing.htm>
9. Fang, H., Baret, F., Plummer, S., & Schaepman-Strub, G. (2019). An overview of global leaf area index (LAI): Methods, products, validation, and applications. *Reviews of Geophysics*, *57*(3), 739–799. <https://doi.org/10.1029/2018RG000608>
10. Filipponi, F. (2018, March). BAIS2: Burned area index for Sentinel-2. In Proceedings (Vol. 2, No. 7, p. 364). MDPI. <https://doi.org/10.3390/ecrs-2-05177>
11. Fu, Y., Tan, X., Yao, Y., Wang, L., Shan, Y., Yang, Y., & Jing, Z. (2024). Uncovering optimal vegetation indices for estimating wetland plant species diversity. *Ecological Indicators*, *166*, 112367. <https://doi.org/10.1016/j.ecolind.2024.112367>



12. Gao, P., Cheng, C., & Song, C. (2019). Satellite Remote Sensing for Biodiversity Conservation: Exemplary practices and lessons learned. *Landscape Ecology*, 34(8), 2045–2047. <https://doi.org/10.1007/s10980-019-00874-z>
13. Gandhi, G. M., Parthiban, S., Thummalu, N., & Christy, A. (2015). NDVI: Vegetation change detection using remote sensing and gis—A case study of Vellore District. *Procedia computer science*, 57, 1199–1210. <https://doi.org/10.1016/j.procs.2015.07.415>
14. Gould W.A. 2000. Remote sensing of vegetation, plant species richness, and regional diversity hotspots. *Ecological Applications* 10: 1861–1870. [https://doi.org/10.1890/1051-0761\(2000\)010\[1861:RSOVPS\]2.0.CO;2](https://doi.org/10.1890/1051-0761(2000)010[1861:RSOVPS]2.0.CO;2)
15. Houlès, V., Guérif, M., & Mary, B. (2007). Elaboration of a nitrogen nutrition indicator for winter wheat based on leaf area index and chlorophyll content for making nitrogen recommendations. *European Journal of Agronomy*, 27(1), 1–11. <https://doi.org/10.1016/j.eja.2006.10.001>
16. Helfenstein, I. S., Schneider, F. D., Schaepman, M. E., & Morsdorf, F. (2022). Assessing biodiversity from space: Impact of spatial and spectral resolution on trait-based functional diversity. *Remote Sensing of Environment*, 280, 113024. <https://doi.org/10.1016/j.rse.2022.113024>
17. Jetz, W., McPherson, J. M., & Guralnick, R. P. (2019). Integrating biodiversity distribution knowledge: Toward a global map of life. *Nature Ecology & Evolution*, 3(5), 391–400. <https://doi.org/10.1016/j.tree.2011.09.007>
18. Lausch, A., Pause, M., Merbach, I., et al. (2018). Linking Earth Observation and taxonomic, structural and functional biodiversity: Local to ecosystem perspectives. *Ecological Indicators*, 38(1), 84–93. <https://doi.org/10.1016/j.ecolind.2016.06.022>
19. Lausch, A., Baade, J., Bannehr, L., Borg, E., Bumberger, J., Chabrilliat, S., Dietrich, P., Gerighausen, H., Glässer, C., Hacker, J., Haase, D., Jagdhuber, T., Jany, S., Jung, A., Karnieli, A., Kraemer, R., Makki, M., Mielke, C., Möller, M., ... Schaepman, M. (2019). Linking remote sensing and geodiversity and their traits relevant to biodiversity—part I: Soil characteristics. *Remote Sensing*, 11(20), 2356. <https://doi.org/10.3390/rs11202356>
20. Lécuyer, L., Alard, D., Calla, S., Coolsaet, B., Fickel, T., Heinsoo, K., Henle, K., Herzon, I., Hodgson, I., Quétier, F., McCracken, D., McMahon, B. J., Melts, I., Sands, D., Skrimizea, E., Watt, A., White, R., & Young, J. (2021). Conflicts between agriculture and Biodiversity Conservation in Europe: Looking to the future by learning from the past. *Advances in Ecological Research*, 3–56. <https://doi.org/10.1016/bs.aecr.2021.10.005>
21. Li, L., Mu, X., Jiang, H., Chianucci, F., Hu, R., Song, W., Qi, J., Liu, S., Zhou, J., Chen, L., Huang, H., & Yan, G. (2023). Review of ground and aerial methods for vegetation cover fraction (fCover) and related quantities estimation: Definitions, advances, challenges, and future perspectives. *ISPRS Journal of Photogrammetry and Remote Sensing*, 198, 1–18. <https://doi.org/10.1016/j.isprsjprs.2023.03.020>
22. Müllerová, J., Kent, R., Brůna, J., Bučas, M., Estrany, J., Manfreda, S., Michez, A., Mokroš, M., Tsiafouli, M. A., & Gago, X. (2025). Understanding spatio-temporal complexity of vegetation



using drones, what could we improve? *Journal of Environmental Management*, 373, 123656.
<https://doi.org/10.1016/j.jenvman.2024.123656>

23. Parviainen, M., Luoto, M., & Heikkinen, R. K. (2010). NDVI-based productivity and heterogeneity as indicators of plant-species richness in boreal landscapes. *Boreal Environment Research*, 15(3), 301–313.
<http://hdl.handle.net/10138/233102>
24. Pereira, H. M., Ferrier, S., Walters, M., Geller, G. N., Jongman, R. H., Scholes, R. J., ... & Wegmann, M. (2013). Essential biodiversity variables. *Science*, 339(6117), 277-278.
[DOI: 10.1126/science.1229931](https://doi.org/10.1126/science.1229931)
25. Pettorelli, N., Schulte to Bühne, H., Tulloch, A., et al. (2018). Satellite remote sensing of ecosystem functions: Opportunities for monitoring biodiversity and evaluating conservation impacts. *Nature Reviews Earth & Environment*, 1(7), 530–546.
<https://doi.org/10.1002/rse2.59>
26. Pettorelli, N., Williams, J., Schulte to Bühne, H., & Crowson, M. (2024). Deep learning and satellite remote sensing for biodiversity monitoring and conservation. *Remote Sensing in Ecology and Conservation*.
<https://doi.org/10.1002/rse2.415>
27. Reddy, C. S. (2021). Remote sensing of biodiversity: What to measure and monitor from space to species? *Biodiversity and Conservation*, 30(10), 2617–2631.
<https://doi.org/10.1007/s10531-021-02216-5>
28. Santangeli, A., Chen, Y., Kluehn, E., Chirumamilla, R., Tiainen, J., & Loehr, J. (2020). Integrating drone-borne thermal imaging with artificial intelligence to locate bird nests on agricultural land. *Scientific Reports*, 10(1).
<https://doi.org/10.1038/s41598-020-67898-3>
29. Schimel, D., & Schneider, F. D. (2019). Flux towers in the sky: Global ecology from space. *New Phytologist*, 224(2), 570–584. <https://doi.org/10.1111/nph.15934>
30. Schulz, C., Förster, M., Vulova, S. V., Rocha, A. D., & Kleinschmit, B. (2024). Spectral-temporal traits in sentinel-1 C-band SAR and sentinel-2 multispectral remote sensing time series for 61 tree species in Central Europe. *Remote Sensing of Environment*, 307, 114162.
<https://doi.org/10.1016/j.rse.2024.114162>
31. Skidmore, A. K., Coops, N. C., Neinavaz, E., Ali, A., Schaepman, M. E., Paganini, M., ... & Wingate, V. (2021). Priority list of biodiversity metrics to observe from space. *Nature Ecology & Evolution*, 5(7), 896-906. [DOI:10.1038/s41559-021-01451-x](https://doi.org/10.1038/s41559-021-01451-x)
32. Torresani, M., Kleijn, D., de Vries, J. P., Bartholomeus, H., Chieffallo, L., Cazzolla Gatti, R., Moudrý, V., Da Re, D., Tomelleri, E., & Rocchini, D. (2023). A novel approach for surveying flowers as a proxy for bee pollinators using drone images. *Ecological Indicators*, 149, 110123.
<https://doi.org/10.1016/j.ecolind.2023.110123>
33. Torresani, M., Rocchini, D., Ceola, G., de Vries, J. P., Feilhauer, H., Moudrý, V., Bartholomeus, H., Perrone, M., Anderle, M., Gamper, H. A., Chieffallo, L., Guatelli, E., Gatti, R. C., & Kleijn, D. (2024). Grassland vertical height heterogeneity predicts flower and Bee Diversity: An UAV



- photogrammetric approach. *Scientific Reports*, 14(1).
<https://doi.org/10.1038/s41598-023-50308-9>
34. Tucker, C. J. (1979). Red and photographic infrared linear combinations for monitoring vegetation. *Remote Sensing of Environment*, 8, 127–150.
[https://doi.org/10.1016/0034-4257\(79\)90013-0](https://doi.org/10.1016/0034-4257(79)90013-0)
35. Turner, W., Rondinini, C., Pettorelli, N., et al. (2018). Free and open-access satellite data are key to biodiversity conservation. *Biological Conservation*, 182(1), 173–176.
<https://doi.org/10.1016/j.biocon.2018.02.008>
36. U.S. Geological Survey. (2018). *NDVI: Foundation of remote sensing phenology*. U.S. Department of the Interior. Retrieved December 12, 2024, from
<https://www.usgs.gov/special-topics/remote-sensing-phenology/science/ndvi-foundation-remote-sensing-phenology#overview>
37. University of North Carolina, Institute for the Environment. (n.d.). *How satellite images are different from photographs*. Retrieved [insert retrieval date], from
<https://ie.unc.edu/wp-content/uploads/sites/277/2014/12/How-Satellite-images-are-different-from-photographs.pdf>
38. Vanbergen, A. J., Aizen, M. A., Cordeau, S., Garibaldi, L. A., Garratt, M. P., Kovács-Hostyánszki, A., ... & Young, J. C. (2020). Transformation of agricultural landscapes in the Anthropocene: Nature's contributions to people, agriculture and food security. In *Advances in Ecological Research* (Vol. 63, pp. 193-253). Academic Press.
<https://doi.org/10.1016/bs.aecr.2020.08.00>
39. Weiss, M. (2016, May 2). *S2ToolBox level 2 products: Lai, FAPAR, FCOVER*. S2ToolBox Level 2 products: LAI, FAPAR, FCOVER Version 2.0.
https://step.esa.int/docs/extra/ATBD_S2ToolBox_V2.0.pdf
40. Westoby, M. J., Brasington, J., Glasser, N. F., Hambrey, M. J., & Reynolds, J. M. (2012). 'Structure-from-Motion' photogrammetry: A low-cost, effective tool for geoscience applications. *Geomorphology*, 179, 300-314.
<https://doi.org/10.1016/j.geomorph.2012.08.021>



Annex

Annex 1. Austria-wide grid-deployments of monitoring techniques in BioMonitor4CAP, 2023-2024

Austria										
Date/Device	AudioMoth	camera trap	eDNA soil sample	GoPro	Merlin	physicochemical	Point-count	Song Meter Micro	Song Meter Mini	UAS
2-Jun-23										1
22-Jun-23	1	1								1
29-Jun-23		1								
20-Jul-23	1		1			1		1	1	
23-Aug-23	1							1	1	
18-Sep-23										1
19-Oct-23			2			2				
8-Mar-24										1
14-Mar-24										1
5-Apr-24										1
3-May-24	2							2		
6-May-24					2		2	2		
23-May-24	3		1		2	1	2	5		
24-May-24			2		1	2	1	1		
25-May-24										1
27-May-24			3			3				
11-Jun-24	3							3		
13-Jun-24					2		2	2		
14-Jun-24					1		1	1		
27-Jun-24	1							1		
28-Jun-24										1
2-Jul-24					1		1	1		
16-Jul-24										1
25-Jul-24		1		1						
23-Aug-24		1		1						
17-Sep-24										1
18-Sep-24										1
20-Sep-24										1
10-Oct-24			1			1				
29-Nov-24										1
Grand Total	12	4	10	2	9	10	9	20	2	13



Annex 2. Bulgaria-wide grid-deployments of monitoring techniques in BioMonitor4CAP, 2023-2024

Bulgaria								
Date/Device	AudioMoth	eDNA soil sample	pan trap	physicochemical	Point-count	Song Meter Micro	transect walk	vane trap
12-Jun-23	1							
13-Jun-23			2				2	
14-Jun-23				2				
20-Jun-23							2	
5-Jul-23	1	2	2					
6-Jul-23							2	
28-Aug-23	1		2				2	
2-Apr-24	4							
3-Apr-24	2				3	2		
4-Apr-24					2			
13-May-24	4	1		1				
14-May-24	2	1		1	3	2	1	1
15-May-24	3	1		1	2		2	1
16-May-24	1	3		3			2	1
17-May-24	1							1
24-Jun-24	1						1	1
25-Jun-24	1					1	1	
26-Jun-24						1	1	1
27-Jun-24	1						1	1
28-Jun-24							1	1
17-Jul-24							1	
18-Jul-24							1	
8-Aug-24	1					2		2
21-Aug-24								2
26-Aug-24							1	
27-Aug-24							1	
Grand Total	24	8	6	8	10	8	24	10



Annex 3. Germany-wide grid-deployments of monitoring techniques in BioMonitor4CAP, 2024

Germany									
Date/Device	AudioMoth	camera trap	eDNA soil sample	Merlin	physicochemical	Point-count	UAS	vane trap	(blank)
6-Mar-24							1		
8-Mar-24							2		
22-May-24							2		
23-May-24							1		
24-May-24	1								
30-May-24	1								
6-Jun-24	2		1		1				
13-Jun-24	2								
19-Jun-24	1	1	1			1			
20-Jun-24	2		2			2		2	
21-Jun-24	1	1	5			5		1	
23-Jun-24	1	1	1			1		1	
3-Jul-24	1								
4-Jul-24	2							2	
5-Jul-24	1	1						1	
7-Jul-24	1	1						1	
8-Jul-24							1	2	
11-Jul-24							3		
17-Jul-24	2								
18-Jul-24	2							2	
19-Jul-24	1	1						1	
21-Jul-24	1	1						1	
22-Jul-24				2		2			
23-Jul-24	1							1	
25-Jul-24				2		2			
29-Jul-24				1		1			
30-Jul-24	1							1	
15-Aug-24			1			1			
16-Aug-24	1							2	
23-Sep-24							1		
25-Sep-24								1	
30-Sep-24							3		
(blank)									1
Grand Total	25	7	11	5		11	5	14	1



Annex 4. Finland-wide grid-deployments of monitoring techniques in BioMonitor4CAP, 2023-2024

Finland										
Date/Device	AudioMoth	camera trap	eDNA soil sample	pan trap	physicochemical	pitfall trap	Point-count	Song Meter Micro	vane trap	vegetation analysis
15-Jun-23	1		1	1		1				
29-Jun-23		1								
29-Apr-24	2							1		
3-May-24	1						2	1		
7-May-24							1			
17-May-24	2							1		
20-May-24	1							1		
3-Jun-24	3	1	2		2			2	2	
4-Jun-24							1			
10-Jun-24							2			
27-Jun-24									1	
1-Jul-24									1	
5-Aug-24		1							1	
9-Aug-24		1								
14-Aug-24		1								
16-Aug-24										1
Grand Total	10	5	3	1	3	1	6	6	5	1

Annex 5. Portugal-wide grid-deployments of monitoring techniques in BioMonitor4CAP, 2024

Portugal					
Date/Device	AudioMoth	eDNA soil sample	physicochemical	Point-count	vane trap
24-Feb-24	1				1
20-Mar-24		1		1	
22-Mar-24	1	2		1	1
1-Apr-24	3	3		3	3
5-May-24				1	
8-May-24	1				1
5-Jun-24	3			3	3
6-Jun-24	1			1	1
8-Oct-24	1				1
10-Oct-24	1				1
17-Oct-24	3				3
Grand Total	15	6	4	10	15



Annex 6. Netherlands-wide grid-deployments of monitoring techniques in BioMonitor4CAP, 2024

Netherlands		
Date/Device	eDNA soil sample	physicochemical
4-Jun-24	1	1
Grand Total	1	1

Annex 7. Peru-wide grid-deployments of monitoring techniques in BioMonitor4CAP, 2023-2024

Peru						
Date/Device	AudioMoth	eDNA soil sample	LAI	pan trap	physicochemical	pitfall trap
1-Aug-23					3	
23-May-24	10					
2-Jun-24	4	4	4	4	4	4
16-Sep-24	2	3		3	3	3
23-Sep-24	1					
Grand Total	17	7	4	7	10	7

Annex 8. Poland-wide grid-deployments of monitoring techniques in BioMonitor4CAP, 2024

Poland	
Date/Device	AudioMoth
(blank)	1
Grand Total	1



Annex 9. UK-wide grid-deployments of monitoring techniques in BioMonitor4CAP, 2024**United Kingdom**

Date/Device	AudioMoth	eDNA soil sample	Song Meter Micro	Song Meter Mini Bat	vane trap
13-May-24			1	1	
19-May-24			1	1	
23-May-24					6
25-May-24	1		1	1	
2-Jun-24	1		1	1	
8-Jun-24	1		1	1	
15-Jun-24	1		1	1	
22-Jun-24	1	1	1	1	
23-Jun-24		5			
30-Jun-24	1		1	1	
17-Jul-24	1		1	1	
21-Jul-24	1		1	1	
31-Jul-24	1		1	1	
1-Aug-24					6
5-Aug-24			1	1	
12-Aug-24	1		1	1	
30-Aug-24	1		1	1	
6-Sep-24	1		1	1	
14-Sep-24	1		1	1	
19-Sep-24					6
21-Sep-24	1		1	1	
29-Sep-24	1		1	1	
Grand Total	15	6	18	18	18



Annex 10. Final selection of biodiversity indicators obtained from Deliverable 1.2. Satellite and drone metrics and indicators are highlighted in bold. Final Scores are indicated out of a maximum value of 15.

EBV Class	EBV Name	Thematic Area	Metrics and Indicators	Final Score
Genetic composition	Genetic differentiation	Insects	DNA barcodes followed (or not) by NGS	14.0
		Soil	Gene sequencing and DNA fingerprints	14.0
Species Population	Species abundance	Birds	Species abundance / Relative species abundance	14.0
		Insects	Species abundance / Relative species abundance	14.0
		Land Cover	Population density / Population biomass	13.0
		Soil	Population density / Population biomass	13.0
	Species distribution	Birds	Species richness (e.g. presence/absence)	14.0
		Insects	Species richness (e.g. presence/absence)	13.0
Soil		Species richness (e.g. presence/absence)	14.0	
Species Traits	Morphology	Land Cover	Specific leaf area	15.0
	Phenology	Land Cover	Species green-up/senescence (start/end of season)	14.0
	Physiology	Land Cover	Leaf dry matter content Chlorophyll content and flux	14.0
Community composition	Community abundance	Insects	Species abundance and related indexes	14.0
		Land Cover	Species abundance and related indexes	13.0
		Soil	Species abundance and related indexes	15.0
	Taxonomic/Phylogenetic diversity	Birds	Species richness and other diversity indices	13.0
		Insects	Species richness and other diversity indices	15.0
		Land Cover	Species richness and other diversity indices	13.0
		Soil	Species richness and other diversity indices	15.0
Ecosystem Function	Ecosystem phenology	Land Cover	Land surface green-up/senescence (start/end season) Peak season (max of season)	15.0
	Primary productivity	Land Cover	Fraction of absorbed photosynthetically active radiation (FAPAR) Specific leaf area Chlorophyll content and flux	15.0
		Soil	Soil moisture	15.0
Ecosystem Structure	Ecosystem distribution	Land Cover	Habitat structure Ecosystem extent and fragmentation Ecosystem structural variance	14.0
	Ecosystem Vertical Profile	Land Cover	Forest species and age Aboveground Biomass Leaf area index Deadwood habitat	14.0
	Live cover fraction	Land Cover	Land cover (vegetation/crop type) Fraction of land cover (vegetation/crop) Canopy cover	14.0



Annex 11. Parameters and Flight Information for March

Parameters	Site & flight information							
	Grid 1						Grid 2 and 3	
Site Name								
Sensor	MicaSense (Altum)			DJI (ZenmuseP1)			MicaSense (Altum)	DJI (ZenmuseP1)
Flight Altitude	30m	60m	120m	30m	60m	120m	120m	120m
Flight Date	20240306	20240306	20240306	20240308	20240306	20240308	20240308	20240308
Mission Number	3	1	2	5	4	6	7	8
Station Altitude from Sea Level	92m	92m	92m	92m	92m	92m	77m	77m
Check of Completeness of Data	Checked	Checked	Checked	Checked	Checked	Checked	Checked	Checked
Time Flight Began	11:54	09:46	10:59	11:38	15:24	13:31	14:56	15:50
Time Flight Ended	14:16	10:29	11:50	13:28	15:48	14:07	15:41	16:35
Percent Overlap of Orthophotos	80%	80%	80%	80%	80%	80%	80%	80%
Pixel Resolution	1.29cm	2.63cm	5.18cm	0.38cm	0.77cm	1.51cm	5.18cm	1.51cm
Time Frequency	4	4	4	4	4	4	4	4
File Type	TIFF	TIFF	TIFF	DNG	DNG	DNG	TIFF	DNG
Coordinate System	WGS 84	WGS 84	WGS 84	WGS 84	WGS 84	WGS 84	WGS 84	WGS 84
Weather Conditions								
Reported Issues								

Annex 12. Parameters and Flight Information for May

Parameters	Site & flight information							
	Grid 1						Grid 2 and 3	
Site Name								
Sensor	MicaSense (Altum)			DJI (ZenmuseP1)			MicaSense (Altum)	DJI (ZenmuseP1)
Flight Altitude	30m	60m	120m	30m	60m	120m	120m	120m
Flight Date	20240524	20240524	20240523	20240523	20240523	20240523	20240522	20240522
Mission Number	7	8	3	6	4	5	1	2
Station Altitude from Sea Level	92m	92m	92m	92m	92m	92m	77m	77m
Check of Completeness of Data	Checked	Checked	Checked	Checked	Checked	Checked	Checked	Checked
Time Flight Began	09:06	11:33	09:04	13:26	12:07	12:46	09:50	11:03
Time Flight Ended	11:07	11:58	09:41	15:15	12:44	13:24	10:36	11:43
Percent Overlap of Orthophotos	80%	80%	80%	80%	80%	80%	80%	80%
Pixel Resolution	1.29cm	2.63cm	5.18cm	0.38cm	0.77cm	1.51cm	5.18cm	1.51cm
Time Frequency	4	4	4	4	4	4	4	4
File Type	TIFF	TIFF	TIFF	DNG	DNG	DNG	TIFF	DNG
Coordinate System	WGS 84	WGS 84	WGS 84	WGS 84	WGS 84	WGS 84	WGS 84	WGS 84
Weather Conditions								
Reported Issues								



Annex 13. Parameters and Flight Information for July

Parameters	Site & flight information									
	Grid 1						Grid 2 and 3		Grid 4	
Site Name										
Sensor	MicaSense (Altum)			DJI (ZenmuseP1)			MicaSense (Altum)	DJI (Zenmuse P1)	MicaSense (Altum)	DJI (ZenmuseP1)
Flight Altitude	30m	60m	120m	30m	60m	120m	120m	120m	120m	120m
Flight Date	20240709	20240709	20240709	20240708	20240708	20240708	20240717	20240711	20240717	20240711
Mission Number	4	5	6	1	2	3	8	7	10	8
Station Altitude from Sea Level	92m	92m	92m	92m	92m	92m	77m	77m	70m	70m
Check of Completeness of Data	Checked	Checked	Checked	Checked	Checked	Checked	Checked	Checked	Checked	Checked
Time Flight Began	09:31	11:33	12:20	11:08	12:56	13:35	08:51	11:38	10:11	13:27
Time Flight Ended	11:30	12:19	12:58	12:52	13:31	14:10	09:31	12:36	10:25	13:39
Percent Overlap of Orthophotos	80%	80%	80%	80%	80%	80%	80%	80%	80%	80%
Pixel Resolution	1.29cm	2.63cm	5.18cm	0.38cm	0.77cm	1.51cm	5.18cm	1.51cm	5.18cm	1.51cm
Time Frequency	4	4	4	4	4	4	4	4	2	2
File Type	TIFF	TIFF	TIFF	DNG	DNG	DNG	TIFF	DNG	TIFF	DNG
Coordinate System	WGS 84	WGS 84	WGS 84	WGS 84	WGS 84	WGS 84	WGS 84	WGS 84	WGS 84	WGS 84
Weather Conditions										
Reported Issues										

Annex 14. Parameters and Flight Information for September

Parameters	Site & flight information									
	Grid 1						Grid 2 and 3		Grid 4	
Site Name										
Sensor	MicaSense (Altum)			DJI (ZenmuseP1)			MicaSense (Altum)	DJI (Zenmuse P1)	MicaSense (Altum)	DJI (Zenmuse P1)
Flight Altitude	30m	60m	120m	30m	60m	120m	120m	120m	120m	120m
Flight Date	20241007	20240923	20240923	20241007	20240923	20240923	20240930	20240930	20240930	20240930
Mission Number	9	4	3	10	2	1	5	6	7	8
Station Altitude from Sea Level	92m	92m	92m	92m	92m	92m	77m	77m	70m	70m
Check of Completeness of Data	Checked	Checked	Checked	Checked	Checked	Checked	Checked	Checked	Checked	Checked
Time Flight Began	07:48	14:26	13:39	14:24	12:25	11:47	09:20	10:31	11:37	12:03
Time Flight Ended	09:49	15:10	14:23	16:06	13:00	12:23	10:04	11:11	11:53	12:17
Percent Overlap of Orthophotos	80%	80%	80%	80%	80%	80%	80%	80%	80%	80%
Pixel Resolution	1.29cm	2.63cm	5.18cm	0.38cm	0.77cm	1.51cm	5.18cm	1.51cm	5.18cm	1.51cm
Time Frequency	4	4	4	4	4	4	4	4	2	2
File Type	TIFF	TIFF	TIFF	DNG	DNG	DNG	TIFF	DNG	TIFF	DNG
Coordinate System	WGS 84	WGS 84	WGS 84	WGS 84	WGS 84	WGS 84	WGS 84	WGS 84	WGS 84	WGS 84
Weather Conditions										
Reported Issues										



Annex 15. Generation of Leaf Area Index (LAI) parameter from Sentinel-2 satellite imagery. This involves loading a region of interest, searching for relevant data, and extracting properties.

```
import rasterio as rio
import planetary_computer
from pystac_client as Client
import numpy as np
import geopandas as gpd

# Date params
date = "2024-05"

# Load region of interest
roi = gpd.read_file(some_roi.geojson)
bbox = roi.union_all().bounds

# Create STAC client from Microsoft Planetary Computer
client = Client.open("https://planetarycomputer.microsoft.com/api/stac/v1/",
modifiers=planetary_computer.sign_inplace)

# Search Sentinel-2 collection
col = client.search(
collections=["sentinel-2-l2a"],
bbox=bbox,
datetime=date
).item_collection()
# Get the first item
item = col[0]
properties = item.properties

# Get parameter
incidence_zenith = properties["s2:incidence_zenith"]
incidence_azimuth = properties["s2:incidence_azimuth"]
mean_solar_zenith = properties["s2:mean_solar_zenith"]
mean_solar_azimuth = properties["s2:mean_solar_azimuth"]

# Bands to get
bands = ["B03", "B04", "B05", "B06", "B07", "B8A", "B11", "B12"]

# Create Sentinel-2 stack image
images = []
for band in bands:
source = rio.open(item.assets[band].href)
image = source.read(1)
images.append(image)

# LAI parameter
layers_parameter = {
"name": "LAI",
"neurons": [
"+ 4.96238030555279 - 0.023406878966470 * b03_norm + 0.921655164636366 * b04_norm +
0.135576544080099 * b05_norm - 1.938331472397950 * b06_norm - 3.342495816122680 * b07_norm +
0.902277648009576 * b8a_norm + 0.205363538258614 * b11_norm - 0.040607844721716 * b12_norm -
0.083196409727092 * viewZen_norm + 0.260029270773809 * sunZen_norm + 0.284761567218845 * relAzim_norm",
"+ 1.416008443981500 - 0.132555480856684 * b03_norm - 0.139574837333540 * b04_norm -
1.014606016898920 * b05_norm - 1.330890038649270 * b06_norm + 0.031730624503341 * b07_norm -
1.433583541317050 * b8a_norm - 0.959637898574699 * b11_norm + 1.133115706551000 * b12_norm +
0.216603876541632 * viewZen_norm + 0.410652303762839 * sunZen_norm + 0.064760155543506 * relAzim_norm",
"+ 1.075897047213310 + 0.086015977724868 * b03_norm + 0.616648776881434 * b04_norm +
0.678003876446556 * b05_norm + 0.141102398644968 * b06_norm - 0.096682206883546 * b07_norm -
1.128832638862200 * b8a_norm + 0.302189102741375 * b11_norm + 0.434494937299725 * b12_norm -
0.021903699490589 * viewZen_norm - 0.228492476802263 * sunZen_norm - 0.039460537589826 * relAzim_norm",
"+ 1.533988264655420 - 0.109366593670404 * b03_norm - 0.071046262972729 * b04_norm +
0.064582411478320 * b05_norm + 2.906325236823160 * b06_norm - 0.673873108979163 * b07_norm -
3.838051868280840 * b8a_norm + 1.695979344531530 * b11_norm + 0.046950296081713 * b12_norm -
0.049709652688365 * viewZen_norm + 0.021829545430994 * sunZen_norm + 0.057483827104091 * relAzim_norm",
"+ 3.024115930757230 - 0.089939416159969 * b03_norm + 0.175395483106147 * b04_norm -
0.081847329172620 * b05_norm + 2.219895367487790 * b06_norm + 1.713873975136850 * b07_norm +
0.713069186099534 * b8a_norm + 0.138970813499201 * b11_norm - 0.060771761518025 * b12_norm +
0.124263341255473 * viewZen_norm + 0.210086140404351 * sunZen_norm - 0.183878138700341 * relAzim_norm"
],
"divide": 3,
"denormalizeValue": [0.000319182538301, 14.4675094548151],
"layer2": "+ 1.096963107077220 - 1.500135489728730 * neuron1 - 0.096283269121503 * neuron2 -
0.194935930577094 * neuron3 - 0.352305895755591 * neuron4 + 0.075107415847473 * neuron5"
}
}
```



```

# Degree to rad
degToRad = np.pi / 180

# Normalizing array
def normalize(arr: np.ndarray, min: float, max: float):
    return 2 * (arr - min) / (max - min) - 1

# Normalizing array
def denormalize(arr: np.ndarray, min: float, max: float):
    return 0.5 * (arr + 1) / (max - min) + min

# Tansig
def tansig(arr: np.ndarray):
    return 2 / (1 + np.exp(-2 * arr)) - 1

# Generated LAI
b03_norm = normalize(images[0], 0, 0.253061520471542)
b04_norm = normalize(images[1], 0, 0.290393577911328)
b05_norm = normalize(images[2], 0, 0.305398915248555)
b06_norm = normalize(images[3], 0.006637972542253, 0.608900395797889)
b07_norm = normalize(images[4], 0.013972727018939, 0.753827384322927)
b8a_norm = normalize(images[5], 0.026690138082061, 0.782011770669178)
b11_norm = normalize(images[6], 0.016388074192258, 0.493761397883092)
b12_norm = normalize(images[7], 0, 0.493025984460231)

viewZen_norm = normalize(np.cos(incidence_zenith * degToRad), 0.918595400582046, 1)

sunZen_norm = normalize(np.cos(mean_solar_zenith * degToRad), 0.342022871159208, 0.936206429175402)

relAzim_norm = np.cos((mean_solar_azimuth - incidence_azimuth) * degToRad)

neurons = layers_parameter["neurons"]
denormalizeValue = layers_parameter["denormalizeValue"]
layer2 = layers_parameter["layer2"]

# Neurons image
for z in range(len(neurons)):
    formula = neurons[z]
    sum = eval(formula)
    globals()[f"neuron{z + 1}"] = tansig(sum)

# Layer final
layer2Image = eval(layer2)

# Denormalize
denormalized = denormalize(layer2Image, *denormalizeValue)

# Check if data need divided
if "divide" in layers_parameter:
    denormalized = denormalized / layers_parameter["divide"]

# LAI data
lai = denormalized

```

